Characterization of a 10 W single-mode Er:Yb doped double-clad fiber laser

A. NIANG[a], F. AMRANI[a], M. SALHI[a], A. KOMAROV[a,b], F. SANCHEZ[a]
[a]*Laboratoire de Photonique d'Angers E.A. 4464, Université d'Angers, 2Bd Lavoisier, 49000 Angers, France*
[b]*Institute of Automation and Electrometry, Russian Academy of Sciences, Acad. Koptyug Pr. 1, 630090 Novosibirsk, Russia*

In this paper we investigate the properties of a 10 W double-clad Er:Yb doped fiber amplifier in two laser setups. It is first studied an all-fibered continuous laser. A laser efficiency of 20 % is obtained with an output power of about 8 W for 40 W pumping power. A passively mode-locked fiber laser is then built up. In the anomalous dispersion regime it is obtained a soliton crystal involving some hundreds of solitons. We demonstrate that the soliton crystal becomes unstable for higher pumping power resulting in its dislocation.

(Received July 2, 2013; accepted July 11, 2013)

Keywords: Fiber laser, Short pulse, cw laser

1. Introduction

Fiber lasers find currently numerous applications spanning from industry, to health and research. The limitations connected to the low output power were overtaken thanks to the breakthrough technology of the double-clad structures and, more recently, of the large mode area fibers. The increase of output power has allowed the achievement of fiber lasers operating either in high power continuous wave (cw) regime, or in Q-switch or mode-locked regimes with even increasing pulse energies. In all cases, due to the single-mode propagation of the lasing signal, the output wave exhibits nearly diffraction-limited beam quality. Although many wavelengths can be generated owing to the large number of radiative transitions in rare earth ions spanning from the visible to infrared range, most of the literature concerns the ytterbium ion which covers the spectral range from 1 µm to 1.2 µm. This is mainly due to the large spectral gain bandwidth together with the very low quantum defect with laser diode pumping at 980 nm resulting in low thermal load compared to other rare earth ions. In cw regime, the ytterbium-doped fiber laser current power performances are above 10 kW with excellent spatial beam quality [1,2]. In the mode-locking regime Yb-doped fibers hold again the record of average output power. Some hundreds of watts can be achieved in the CPA (Chirped Pulse Amplification) architecture [3] while only few ten watts are obtained with a single oscillator with photonic crystal fiber with very large mode area [4]. The CPA architecture consists in a low power oscillator amplified in several stages. In the 1.5 µm eye-safe window, erbium has been less studied in double-clad or large mode area (LMA) fibers combined with high pumping powers. In the cw regime it has been reported output powers of few watts using double-clad fibers with standard core dimension [5,6]. Higher output powers have been obtained using LMA fibers [7] or LMA Yb-free fibers with quasi resonant pumping [8]. Passively mode-locked erbium-doped fiber lasers have been extensively investigated with conventional fibers (single clad) but narrowly with double-clad fibers. In the former case, the soliton fiber laser has been realized in several optical configurations using different mode-locking mechanisms [9]. We were pioneering in the latter case where we demonstrated passive mode-locking in the anomalous dispersion regime with a 1 W double-clad Er:Yb codoped amplifier (maximum available pump power of 7 W) [10,11].

The aim of this paper is to characterize a 10 W Er:Yb codoped double-clad fiber amplifier in different laser configurations. In section II we consider the continuous wave operation in an all-fibered experimental configuration. It is demonstrated that the output power is about 8 W which is currently a record for non LMA double-clad fibers. The 10 W amplifier is then used in a passively mode-locked optical configuration. Experimental results are presented in section III. It is shown that in the anomalous dispersion regime the laser emits a large soliton crystal [12] which undergoes an instability when the pumping power is increased.

2. CW fiber laser

The experimental setup is shown in Fig. 1. It is an all-fibered unidirectional ring cavity with a 10 W Er:Yb codoped amplifier manufactured by KEOPSYS and specially designed for our applications. The amplifier consists in 5 m long double-clad Er:Yb codoped fiber. The geometry of the inner clad has an octagonal shape which allows a high coupling efficiency of the multimode pump wave into the fiber. The diameter of the inner clad is 130 µm and the fiber core diameter is 12 µm. It is pumped at

980 nm with several laser diodes injected with the v-groove technique. The maximum available pumping power is up to 40 W which ensures a total output power of the ASE (Amplified Spontaneous Emission) up to 10 W. This value coincides with the maximum achievable output power in continuous lasing operation. The two fiber ends of the double-clad fiber are spliced to pieces of standard single-mode fibers (SMF 28). The cavity is then realized by connecting the output port of the amplifier with its input. The cavity contains also an optical isolator ensuring a unidirectional oscillation in order to avoid Brillouin backscattering which could damage the fiber through intense acoustic waves [13,14]. The output fiber coupler is placed just at the output of the amplifier. The output coupling coefficient will be varied to optimize the output power.

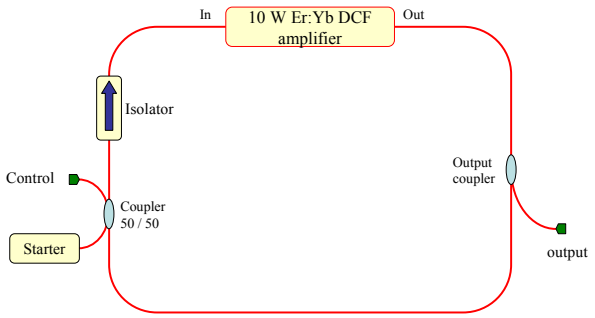

Fig. 1. Experimental setup for the cw laser.

Because of internal electronic security to avoid irreversible damages of the 10 W amplifier in the absence of input signal, an auxiliary laser must be used to start up the amplifier. The external light is launched with a 50/50 coupler to the principal cavity with a signal power of 17 dBm. After the principal laser is operating, we turn-off the starting laser to avoid any slave – master coupling between the two lasers. In fact, the external laser is another home-made Er:Yb doped double-clad fiber laser which is tunable. The cavity is totally fibered thus avoiding any thermal effects at the fiber ends.

In the first series of experiments the output coupling is 10 %. Because the amplifier does not support an external modulation, the lasing effect cannot be evidenced with the simplest way which consists to modulate the pumping power with a square signal thus leading to the observation of the classical relaxation oscillations [15]. The observation of the temporal trace does not allow distinguishing between the amplified spontaneous emission (below the lasing threshold) and the laser signal (above threshold). A clear signature is however delivered by the low frequency spectrum (Fourier transform of the output intensity). Indeed, below the lasing threshold the low frequency spectrum does not exhibit a characteristic frequency while one frequency appears above threshold [16]. It is the one associated to the relaxation oscillations and it can be observed without external modulation since the noise is sufficient to excite it. Figure 2 shows an example of the low frequency spectrum of the laser. The peak at about 45 kHz is characteristic of the relaxation oscillation frequency ω_r (eigenfrequency of the laser) and definitely proves that the laser operates above threshold.

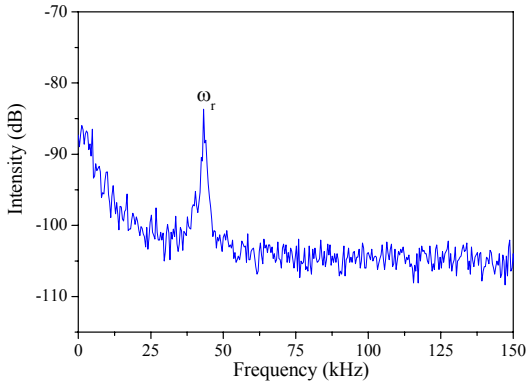

Fig. 2. Low frequency spectrum of the fiber laser for a pumping power of 4 W.

It is has been established that the square of the relaxation oscillation frequency is a linear function of the pumping power [16]. The evolution of ω_r^2 is shown in Fig. 3 and, as expected, it exhibits a linear evolution versus the pumping. The points are the experimental data while the solid line is a linear fit. The intersection of the straight line with the x-axis gives the value of the pumping power at laser threshold. In our case, the threshold is $P_{th} \approx 2.3\,W$.

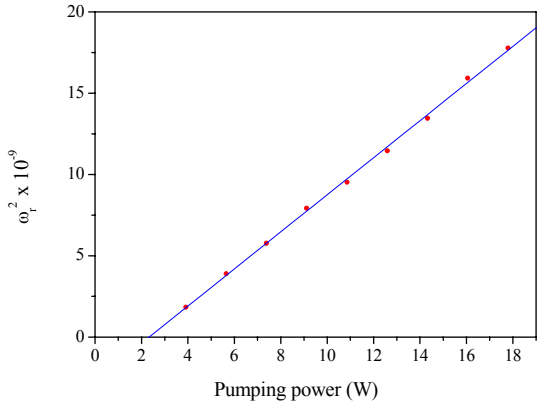

Fig. 3. Evolution of the square of the eigenfrequency versus the pumping power.

The optical spectrum is represented in Fig. 4. For comparison, it is represented in the same plot, the amplified spontaneous emission (ASE) spectrum. We observe that the laser frequency is located in the longer wavelengths range (λ = 1568 nm) of the ASE spectrum thus revealing that the signal undergoes a re-absorption for

short wavelengths. This is probably due to the existence of a part of the doped fiber in which the population inversion is not realized thus favouring absorption at short wavelengths [17].

Let us now consider the output coupling optimization. For that we have tested two output coupling values T = 50% and T = 70%. The 10% output has not been used since the optimization in fiber lasers occurs for high output coupling [20]. Results are summarized in Fig. 5 which gives the evolution of the output power as a function of the pump power. The laser characteristics are linear and the threshold is about 2.5 W in both cases. The fact that the threshold is not very sensitive to the output coupling coefficient means that the losses due to this coupling are low in comparison to other losses of the cavity (distributed and localized). The highest efficiency η is obtained for T = 70 % for which $\eta = 20\%$ while $\eta = 14\%$ for T = 50%. These results are in good agreement with what is usually observed in fiber lasers [20]. In fact the optimum output coupling is certainly above 90 % [21] but such high value will lead to a reinjected signal at the input port of the amplifier below the required value and this is why we did not use a 90% output coupling.

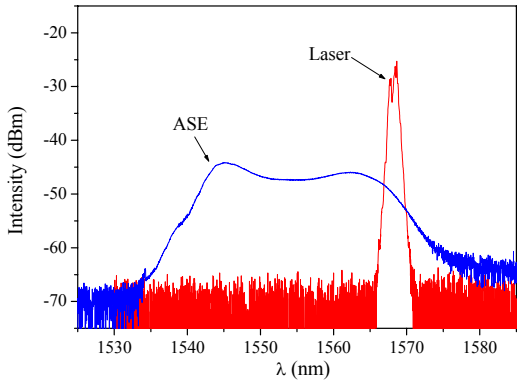

Fig. 4. Optical spectra of both the laser and the amplified spontaneous emission (ASE).

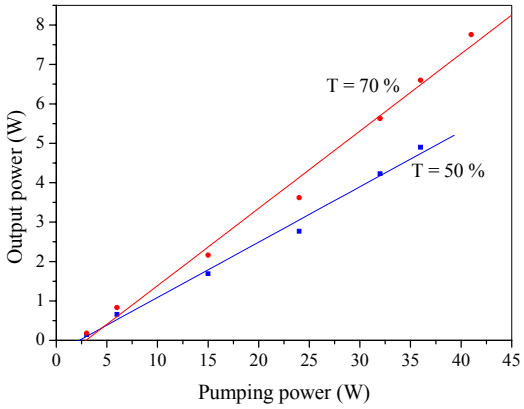

Fig. 5. Evolution of the output power versus the pumping power for two output couplings. Symbols are experimental points and lines correspond to linear fits.

3. Passively mode-locked fiber laser

In this section we consider the passive mode-locking of the laser. Mode locking is achieved through nonlinear polarization rotation technique [22]. The experimental setup is shown in Fig. 6. We use the Er:Yb 10 W fiber amplifier operating at λ = 1.55 µm presented in the previous section. It consists in a 5m long double-clad fiber (DCF) that has a chromatic dispersion coefficient $\beta_2^{DCF} = -0.021\ ps^2/m$. The fibers DCF and SMF 28 operate in the anomalous dispersion regime. A piece of dispersion-shifted fiber ($\beta_2^{DSF} = 0.14\ ps^2/m$) is added to control the total cavity dispersion. To favor multiple-pulse mode locking [23], the total dispersion is set in the anomalous regime with $\beta_2^{TOT} L = -0.12\ ps^2$, with a total cavity length of 30.5 m corresponding to a round trip time of T = 152.9 ns. A polarizing isolator is set between two polarization controllers. Mode locking is obtained through the adjustment of the polarization controllers. The output intensity is detected with a high-speed photodetector (TIA-1200) and visualized with a fast oscilloscope (Tektronix TDS 6124C, 12 GHz, 40 GSa). The spectral properties are analyzed with an optical spectrum analyzer (Anritsu MS 9710C) and the pulse duration is measured with an optical autocorrelator with a scanning range of ±100 ps (Femtochrome FR-103 XL).

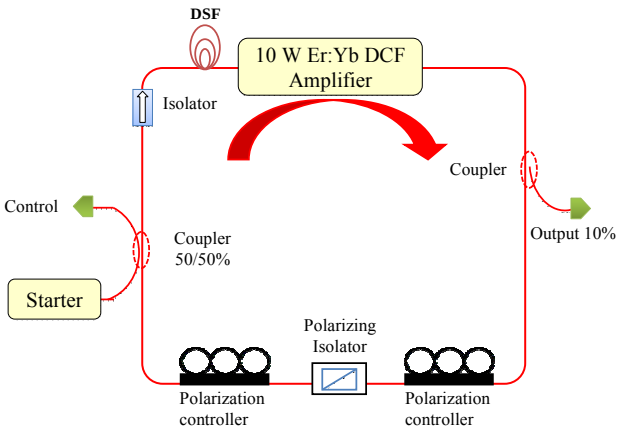

Fig. 6. Experimental setup for the mode-locking operation of the fiber laser.

At moderate pumping power (10W) and adjusting the polarization controllers, a condensate state is formed: it consists in a large number of regularly spaced identical solitons with constant relative phase differences from one round trip to the next. It is a soliton crystal of several hundreds of solitons [11,12]. The soliton train spans over 6.6 ns, as indicated by the temporal intensity recorded in Fig. 7. Note that the resolution of the oscilloscope does not allow separating the pulses and only the temporal envelope is visible. The corresponding optical spectrum given in Fig. 8 proves the strong coherence between pulses since it is modulated with a contrast exceeding 90%. The spectral

period is 0.83 nm, which corresponds to a temporal separation of about 10 ps between solitons, in good agreement with the autocorrelation trace shown in Fig. 9. The latter also proves that the solitons are identical and equidistant. From the train duration and the delay between solitons, we estimate the number of pulses in the soliton crystal to be 660 pulses which is actually a record in comparison to our previous works [11,12].

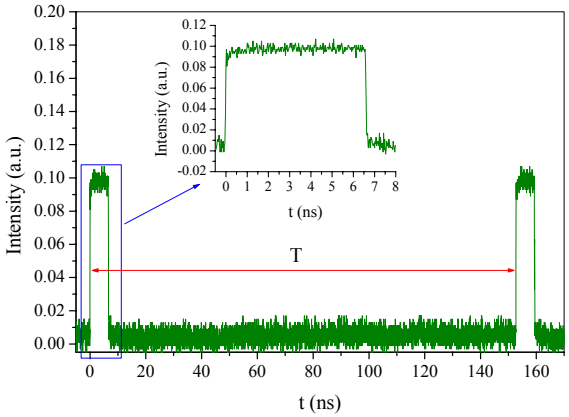

Fig. 7. Temporal trace of a soliton crystal obtained for a pumping power of 10 W.

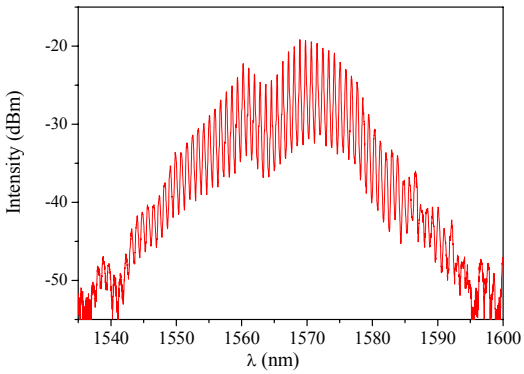

Fig. 8. Optical spectrum of the soliton crystal of Fig. 7.

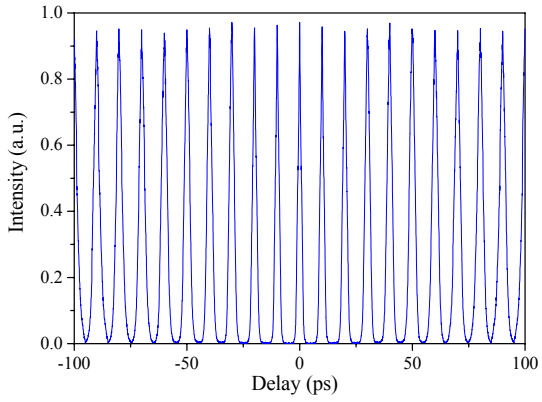

Fig. 9. Autocorrelation trace of the soliton crystal of Fig. 7.

In a previous paper we have theoretically predicted that the number of pulses in the crystal should increase if the pumping power increases [24]. More precisely, the crystal extent should grow while the delay between pulses remains constant. What happens in real experiment? First of all if we increase the pumping power from 10 W to 15 W, the extent of the soliton crystal increases from 6.6 ns to 9.3 ns as it is demonstrated by the temporal intensity recorded in Fig. 10 and in good agreement with [24]. The strongly modulated optical spectrum (not given here) proves the strong coherence between pulses since it is modulated with a contrast exceeding 95%, slightly greater than that of the 6.6 ns soliton crystal. The spectral period is 0.83 nm, which corresponds to a temporal separation of 10 ps between solitons, in good agreement with the autocorrelation trace (not reported here). From the train duration and the delay between solitons, we estimate the number of pulses in the soliton crystal to be 930 pulses. Hence, the increase of the pumping power has led to an increase of the size of the soliton crystal together with a stronger spectral modulation contrast. However, there is no effect on the temporal separation between pulses.

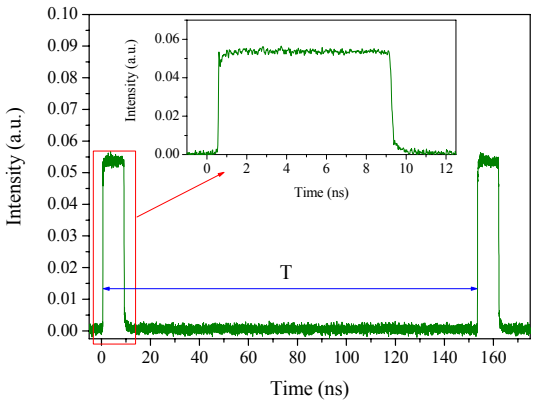

Fig. 10. Temporal trace of a soliton crystal obtained for a pumping power of 15 W.

By increasing again the pump power from 15 W to up to 25W, several soliton packets begin to get loose from the initial soliton crystal. These packets of pulses tend to go away from the initial train of pulses. The evolution is given in Fig. 11. Therefore, when the pumping is increased, the crystal extent first grows and then the crystal undergoes a dislocation resulting in a splitting into different parts. In contrast with the theoretical predictions [24], the crystal extent does not increase for high pumping powers but rather it suffers from an intrinsic instability. The physical reason of this instability is not yet understood.

Just when several soliton packets begin to get loose from the initial soliton crystal a cw component appears in the optical spectrum. The cw component introduces a repulsive force between solitons (or between packets of solitons). Gradually, the soliton packets spread over a large part of the cavity and finally fill the whole cavity as displayed in Fig. 12. The zoom of Fig. 12 reveals that the packets are uniformly distributed and that all packets have

the same time duration. Each packet is a bound state as demonstrated by the strongly modulated optical spectrum of Fig. 13. The spectral period is 0.82 nm resulting in a delay between solitons inside the bound state of 10 ps as confirmed by autocorrelation measurements. The envelope of the autocorrelation trace is nearly triangular which proves that the solitons are identical inside a packet. From the delay and the duration of a bound state we estimate the number of solitons inside a bound state to be about 50. The bound state is therefore a soliton crystal containing only a small part of the total soliton set. We obtain finally the 50th harmonic of soliton crystals containing about 50 solitons [25]. The total number of solitons is therefore about 2500. The optical spectrum of Fig. 13 leads to the following remarks. Firstly, the modulation characterizes the bound state, and secondly the harmonic mode-locking (HML) is correlated with the existence of a cw component visible in the optical spectrum as it was previously indicated [26,27]. The HML state is stable over several hours and is reproducible.

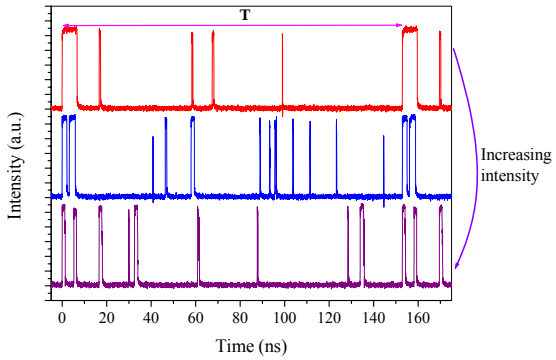

Fig. 11. Evolution of the laser output intensity for increasing pumping powers.

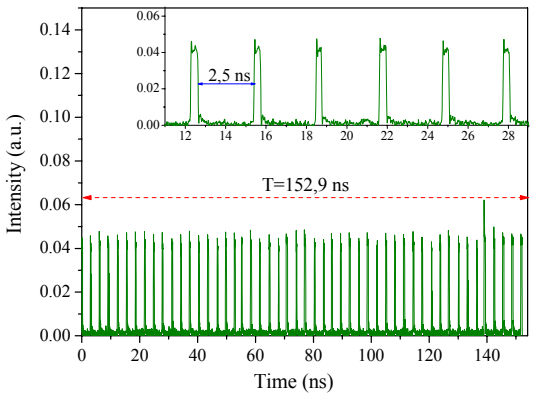

Fig. 12. Temporal trace of harmonic mode-locking of soliton crystals.

4. Conclusion

In summary, we have used a specially designed 10 W Er:Yb fiber amplifier in two optical configurations. The doped fiber is a double-clad fiber with a single-mode core with standard dimensions in contrast with large mode area fibers. We have first realized a continuous operating laser. The laser delivers about 8 W with an efficiency of about 20 % which is currently a record. Better performances are expected with higher output coupling coefficients. The laser is compact, all-fibered and exhibits a diffraction-limited beam quality. On the other hand, we have built a passively mode-locked laser based on the nonlinear polarization rotation technique. Again, the laser is all-fibered in order to avoid thermal effects especially at the silica / air interfaces. The total cavity dispersion has been set in the anomalous dispersion regime in order to favour multiple pulsing. At moderate pumping power and with a suitable orientation of the polarization controllers we have obtained a soliton crystal. A soliton crystal is a particular soliton distribution involving identical and equidistant pulses which have a strong mutual coherence. When the pump power is increased, the soliton crystal first grows and then a dislocation occurs. Our results thus demonstrate that a soliton crystal of large extent suffers from an intrinsic instability whose origin is not yet understood. The final soliton distribution is the harmonic mode-locking of reduced soliton crystal. In order to give some physical insight it will be necessary to carefully investigate the mechanism of dislocation.

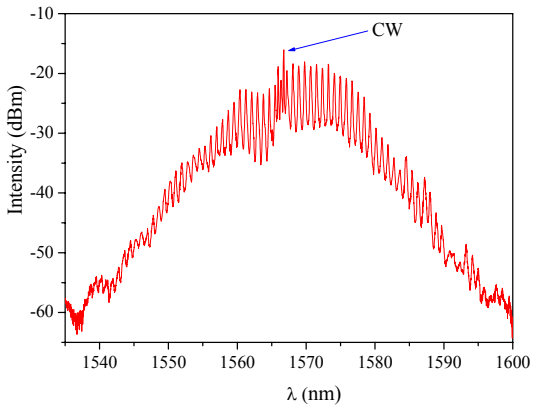

Fig. 13. Optical spectrum of harmonic mode locking of solitons crystal.

References

[1] A. Tunnërmann, T. Schreiber, J. Limpert, Appl. Optics **49**, F71 (2010).
[2] D.J. Richardson, J. Nilsson, W.A. Clarkson, J. Opt. Soc. Am. B **27**, B63 (2010).
[3] T. Eidam, S. Hanf, E. Seise, T.V. Anderson, T. Gabler, C. Wirth, T. Schreiber, J. Limpert, A. Tunnërmann, Opt. Lett. **35**, 94 (2010).
[4] M. Baumgartl, C. Lecaplain, A. Hideur, J. Limpert, A. Tünnermann, Opt. Lett. **37**, 1640 (2012).
[5] M. Salhi, H. Leblond, F. Sanchez, Opt. Com. **247**, 181 (2005).

[6] J. Nilsson, W.A. Clarkson, R. Selvas, J.K. Sahu, P.W. Turner, S.-U. Alam, A.B. Grudinin, Opt. Fiber Technol. **10**, 5 (2004).
[7] Y. Jeong, S. Yoo, C.A. Codemard, J. Nilsson, J. K. Sahu, D. N. Payne, R. Horley, P.W. Turner, L. Hickey, A. Harker, M. Lovelady, A. Piper, IEEE J. Sel. Top. Quant. Electron. **13**, 573 (2007).
[8] J. Zhang, V. Fromzel, M. Dubinskii, Opt. Exp. **19**, 5574 (2011).
[9] M.E. Fermann,A. Galvanauskas, G. Sucha, D. Harter, Appl. Phys. **B 65**, 259 (1997).
[10] A. Haboucha, A. Komarov, H. Leblond, M. Salhi, F. Sanchez, J. Optoelectron. Adv. Mater. **10**, 164 (2008).
[11] A. Haboucha, H. Leblond, M. Salhi, A. Komarov, F. Sanchez, Opt. Lett. **33**, 524 (2008).
[12] A. Haboucha, H. Leblond, M. Salhi, A. Komarov, F. Sanchez, Phys. Rev. **A 78**(12) 043806 (2008).
[13] A. Hideur, T. Chartier, C. Özkul, F. Sanchez, Opt. Com. **186**, 311 (2000).
[14] M. Salhi, A. Hideur, T. Chartier, M. Brunel, G. Martel, C. Özkul, F. Sanchez, Opt. Lett. **27**, 1294 (2002).
[15] M. Le Flohic, P.L. François, J.Y. Allain, F. Sanchez, G. Stephan, IEEE Jour. Quant. Elect. **QE 27**, 1910 (1991).
[16] F. Sanchez, G. Stephan, Phys. Rev. **E 53**, 2110 (1996).
[17] P. Urquhart, IEE Proc. **135 Pt. J**, 385 (1988).
[18] W. W. Rigrod, J. Appl. Phys. **34,** 2602 (1963).
[19] W. W. Rigrod, J. Appl. Phys. **36,** 2487 (1965).
[20] F. Sanchez, B. Meziane, T. Chartier, P.L. François, G.M. Stephan, Appl. Opt. **34**, 7674 (1995).
[21] A. Hideur, T. Chartier, C. Özkul, F. Sanchez, Opt. Lett. **26**, 1054 (2001).
[22] A. Komarov, K. Komarov, D. Meshcheriakov, F. Amrani, F. Sanchez, Phys. Rev. **A 82**(14), 013813 (2010).
[23] A. Komarov, H. Leblond, F. Sanchez, Phys. Rev. **A71**(9), 053809 (2005).
[24] A. Komarov, A. Haboucha, F. Sanchez, Opt. Lett. **33**, 2254 (2008).
[25] F. Amrani, A. Niang, M. Salhi, H. Leblond, F. Sanchez, Opt. Lett. **36**, 4239 (2011).
[26] F. Amrani, A. Haboucha, M. Salhi, H. Leblond, A. Komarov, Ph. Grelu, F. Sanchez, Opt. Lett. **34**, 2120 (2009).
[27] Z. X. Zhang, L. Zhan, X. X. Yang, S. Y. Luo, Y. X. Xia, Laser Phys. Lett. **4**, 592 (2007).

*Corresponding author: francois.sanchez@univ-angers.fr